THE STUDY OF FUSION AND QUASI-ELASTIC REACTIONS SIMULTANEOUSLY

A.M. Izadpanah[†], V. Zanganeh, A. Sadeghloo

Department of Physics, Golestan University
Shahid Beheshti st., P.O. Box 155, Gorgan, Iran

Received 17 August 2025, accepted 30 December 2025, published online 17 February 2026

To investigate the role of surface energy coefficients, we perform a comparative study of heavy-ion fusion and quasi-elastic scattering reactions simultaneously. The results show that the surface energy coefficient significantly influences both fusion and quasi-elastic reactions. Our findings reveal that proximity potential based on the 1977 version, with parameters $\gamma_0 = 1.08948$ MeV/fm^2 and $k_s = 1.9830$, successfully reproduces the experimental measurements of fusion and quasi-elastic scattering. The average relative errors for the fusion cross section and quasi-elastic scattering data for selected reactions are 0.0558 and 0.0826, respectively.

DOI:10.5506/APhysPolB.57.3-A1

1. Introduction

In recent years, extensive experimental and theoretical efforts have been made to study the synthesis of superheavy nuclei through heavy-ion reactions. For this purpose, numerous theoretical and experimental studies have been performed on fusion and quasi-elastic scattering reactions [1, 2]. Determining the exact interaction potential between two nuclei is challenging and requires ongoing research in this area.

From the perspective of quantum tunneling, quasi-elastic scattering (a process that includes non-elastic scattering, transfer a small number of nucleons, and energy exchange) is a suitable counterpart to heavy-ion fusion reactions [3–5]. This is because quasi-elastic scattering depends on the probability of reflection from the potential barrier, while fusion depends on the probability of penetration through it. Furthermore, using experimental values of the fusion excitation function and larg-angle quasi-elastic scattering data, a similar barrier distribution (resulting from the coupling of internal degrees of freedom with the relative motion of the projectile

[†] Corresponding author: a.izadpanah@gu.ac.ir

and target system) can be achieved [6]. Therefore, a unified description of these cross sections near the Coulomb barrier is expected when using the same nucleon–nucleon potential. In 2008, Wang and Scheid [7] showed that using the Woods–Saxon potential and considering the experimental fusion barrier distribution for spherical nuclear reactions, both fusion and quasi-elastic scattering can be explained simultaneously; this potential also predicts quasi-elastic cross sections for reactions lacking experimental data.

In recent years, the surface diffuseness anomaly has attracted considerable attention in heavy-ion fusion and scattering research [8, 9]. However, the effects of nuclear matter incompressibility, which are crucial in fusion reactions, are not accounted for in this potential [10]. In many studies on nuclear reactions, the proximity potential has been employed, providing a robust test and support for microscopic and macroscopic models of fusion reactions [11–14].

In our previous work [15], we evaluated the performance of fourteen different proximity model versions in simultaneously reproducing fusion and quasi-elastic cross sections. That study demonstrated that the proximity potential 1977 (Prox77) and its modified version (Mod. Prox77) can accurately estimate the cross sections of both phenomena. In this paper, we extend our previous work to simultaneously calculate fusion and quasi-elastic scattering for different values of the surface energy constant and surface asymmetry constant parameters, investigating the influence of these parameters with greater precision. For this purpose, we will examine the role of the surface energy constant and the surface asymmetry constant.

The article is structured as follows. Section 2 reviews the proximity potential. In Section 3, we introduce the method for calculating the fusion cross section using barrier distribution and investigate quasi-elastic scattering using the same concept. Sections 4 and 5 present the results and discussion, and the summary and conclusions, respectively.

2. Description of the interacting potential model

The proximity potential is based on the following concept: "The force between two slightly curved surfaces in close proximity is proportional to the interaction potential per unit area between two flat surfaces". According to the original version, known as the proximity potential 1977 [10], the nuclear interaction potential between two surfaces $V_{\mathrm{N}}(r)$ is given by

$$V_{\mathrm{N}}(r) = 4\pi\gamma b\bar{R}\Phi\left(\frac{r - C_1 - C_2}{b}\right)\ \mathrm{MeV}\,. \tag{1}$$

Here, $\bar{R}$ is the mean curvature radius, defined as

$$\bar{R} = \frac{C_1 C_2}{C_1 + C_2}\,, \tag{2}$$

where C_i represents the half-density radius of curvature of the nuclei, given by

$$C_i = R_i \left[1 - \left(\frac{b}{R_i}\right)^2 + \ldots\right], \tag{3}$$

and R_i is the effective nuclear radius

$$R_i = 1.28\, A_i^{1/3} - 0.76 + 0.8\, A_i^{-1/3} \text{ fm} \qquad (i = 1,\, 2)\,. \tag{4}$$

In Eq. (1), $\Phi(x_i = \frac{r - C_1 - C_2}{b})$ is a universal function that depends on the separation distance between the surfaces of the two interacting nuclei. Unlike $\bar{R}$ and ϕ, which are independent of isospin, the surface energy coefficient γ in Eq. (2) is related to the neutron and proton excess through

$$\gamma = \gamma_0 \left[1 - k_{\rm s} \left(\frac{N - Z}{N + Z}\right)^2\right], \tag{5}$$

where N and Z are the total numbers of neutrons and protons, $k_{\rm s}$ is the surface asymmetry constant, and γ_0 is the surface energy constant. In this version, γ_0 and $k_{\rm s}$ are 0.9517 MeV/fm^2 and 1.7826, respectively. For a symmetrically interacting pair of nuclei (*i.e.*, $N = Z$), $\gamma = \gamma_0 = 0.9517$ MeV/fm^2.

When $(\frac{N-Z}{N+Z}) = 0.5$, γ reduces to 0.5276 MeV/fm^2. Defining the asymmetry parameter $A_s = [\frac{N_1+N_2-(Z_1+Z_2)}{N_1+N_2+(Z_1+Z_2)}]$, a sharp decrease in the potential is observed for asymmetric colliding pairs. Different versions of the proximity potential are obtained by using various surface tension parameters γ [16, 17]. Assuming ξ as the minimum separation distance in units of the surface width, the universal function $\Phi(\xi)$ in Prox77 is parameterized as

$$\Phi(\xi) = \begin{cases} -\frac{1}{2}\,(\xi - 2.54)^2 - 0.0852\,(\xi - 2.54)^3 & \text{for } \xi \le 1.2511\,, \\ -3.437\exp\left(-\xi/0.75\right) & \text{for } \xi \ge 1.2511\,. \end{cases} \tag{6}$$

Using the above equations, the nuclear part of the interaction potential $V_{\rm N}(r)$ can be calculated. This model is referred to as Prox77.

Modified versions of Prox77 were introduced based on adjustments to the surface energy coefficient [15]. Table 1 presents the 12 different subversions of Prox77 used in this work.

Table 1. The modified versions of the Prox77.

	γ_0 [MeV/fm^2]	k_s	Ref.
Subversion 1	1.01734	1.79	[31]
Subversion 2	1.460734	4.0	[32]
Subversion 3	1.2402	3.0	[33]
Subversion 4	1.1756	2.2	[34]
Subversion 5	1.27326	2.5	[34]
Subversion 6	1.2502	2.4	[34]
Subversion 7	0.9517	2.6	[35]
Subversion 8	1.2496	2.3	[36]
Subversion 9	1.25284	2.345	[37]
Subversion 10	1.08948	1.9830	[38]
Subversion 11	0.9180	0.7546	[38]
Subversion 12	0.911445	2.2938	[38]

Another version, called the Generalized Proximity 1977 (Gen. Prox77), was introduced by defining the universal function as:

$$\phi(s) = \begin{cases} -1.7817 + 0.927\,s + 0.0169\,s^2 - 0.05148\,s^3 & \text{for } 0 \le s \le 1.9475\,, \\ -4.41\exp\left(-s/0.7176\right) & \text{for } s > 1.9475 \end{cases} \tag{7}$$

using the same constants as in Prox77. In this version, the radii R_{0i} are defined as

$$R_{0i} = r_i - \frac{b^2}{r_i}\ \text{fm}\,, \tag{8}$$

where $r_i = 1.28A_i^{1/3} + 0.8A_i^{-1/3} - 0.76$ and $b = 0.99$ fm.

Other versions of the proximity potential can be found in Refs. [18–30].

3. Calculation of fusion and quasi-elastic cross sections considering barrier distribution

For spherical interacting nuclei, only a single potential barrier is encountered (the SBPM model). However, if we consider more realistic, deformed nuclei, interacting nuclei collide with a distribution of potential barriers. Deformed nuclei experience a broader barrier distribution due to additional degrees of freedom, such as vibration and rotation.

By obtaining the experimental barrier distribution, virtually all degrees of freedom are accounted for, providing an accurate representation of the nuclear potential. The experimental barrier distribution, obtained by taking the second numerical derivative of the product of the cross section and energy with respect to the center-of-mass energy, serves as a reliable metric for assessing the accuracy of theoretical methods and potentials. Here, we compare the accuracy of different proximity potential versions by examining their predicted barrier distributions against experimental data. In this method, the fusion cross section is calculated based on the penetration model of a real multidimensional barrier using the following relation [41, 42]:

$$\sigma_{\rm fus}(E_{\rm cm}) = \int_0^\infty D(B)\sigma^1_{\rm fus}(E_{\rm cm}, B){\rm d}B\,, \tag{9}$$

where $\sigma^1_{\rm fus}$ is the well-known Wong model

$$\sigma^1_{\rm fus}(E_{\rm cm}, B) = \frac{\hbar\omega R^2_{\rm fus}}{2\,E_{\rm cm}} \ln\left(1 + \exp\left[\frac{2\,\pi}{\hbar\omega}\,(E_{\rm cm} - B)\right]\right)\,. \tag{10}$$

In the above equation, $E_{\rm cm}$ denotes the center-of-mass energy, while B, $R_{\rm fus}$, and $\hbar\omega$ represent the barrier height, radius, and curvature, respectively. These quantities can be calculated by fitting the fusion barrier to a parabolic approximation. A decrease in barrier curvature increases the fusion cross section, whereas an increase in barrier height reduces the probability of tunneling, thereby decreasing the fusion cross section. $D(B)$ is a normalized weight function describing the barrier height distribution. Here, $D(B)$ is derived directly from fusion excitation functions using the second derivative of $E\sigma_{\rm fus}$ with respect to energy

$$D(B) = \frac{1}{\pi\,R_2(E)}\frac{{\rm d}^2(E\sigma)}{{\rm d}E^2}\,. \tag{11}$$

Substituting experimental fusion cross-section values yields the experimental barrier distribution, which can be modeled as a sum of Gaussian functions. Assuming the weight function is described by two Gaussians, $D_1(B)$ and $D_2(B)$ [41, 42]

$$D_1(B) = \frac{\sqrt{\gamma}}{2\,\sqrt{\pi}\,b_1}\exp\left[-\gamma\frac{(B - B_1)^2}{(2\,b_1)^2}\right] \tag{12}$$

and

$$D_2(B) = \frac{1}{2\,\sqrt{\pi}\,b_2}\exp\left[-\frac{(B\,-\,B_2)^2}{(2\,b_2)^2}\right] \tag{13}$$

with

$$b_1 = \frac{1}{4}(B_0 - B_c)\,, \tag{14}$$

$$b_2 = \frac{1}{2}(B_0 - B_c)\,, \tag{15}$$

$$B_1 = B_c + b_1\,, \tag{16}$$

$$B_2 = B_c + b_2\,. \tag{17}$$

Here, B_0 is the fusion barrier height, and $B_c = f\,B_0$ is the effective experimental barrier height, accounting for coupling effects such as dynamic deformation. The optimal reduction factor f is set to 0.922 for Prox77 [15]. The effective weight function $D_{\rm eff}$ is defined as

$$D_{\rm eff} = \begin{cases} D_1(B) & \text{for } B < B_x\,, \\ D_{\rm avg}(B) & \text{for } B \geq B_x\,, \end{cases} \tag{18}$$

where

$$D_{\rm avg}(B) = \frac{D_1(B) + D_2(B)}{2}\,,$$

and B_x is the intersection point of D_1 and $D_{\rm avg}$. As seen from these equations, the peak and width of $D_{\rm eff}(B)$ depend primarily on the barrier height B_0, except for the γ factor in $D_1(B)$, which accounts for nuclear structure effects. In Eqs. (12) and (13), $D(B)$ are weighting functions that incorporate coupling effects such as deformation, vibration, and transfer. For fusion reactions involving nuclei near the stability line (without closed shells) and for energies near and above the barrier, we set $\gamma = 1$. The average barrier height $B_m = \frac{\int B D_{\rm eff}(B){\rm d}B}{\int D_{\rm eff}(B){\rm d}B}$, the most probable barrier height $B_{\rm mp}$, and the full width at half maximum (FWHM) can be readily obtained from $D_{\rm eff}(B)$.

As previously mentioned, large-angle quasi-elastic scattering data can be reproduced using the barrier distribution function derived for fusion reactions [43, 44]. Using $D_{\rm eff}$ at energies near the Coulomb barrier, we have [7]

$$\frac{{\rm d}\sigma_{\rm qel}}{{\rm d}\sigma_{\rm R}}(E_{\rm cm}) = \frac{1}{F_0}\int_0^\infty D_{\rm eff}(B)\frac{{\rm d}\sigma_{\rm el}}{{\rm d}\sigma_{\rm R}}(E_{\rm cm}, B){\rm d}B + P_{\rm corr}\,, \tag{19}$$

where F_0 is the normalization constant given by $F_0 = \int_0^\infty D_{\rm eff}(B){\rm d}B$, and $\frac{{\rm d}\sigma_{\rm el}}{{\rm d}\sigma_{\rm R}}$ is the ratio of elastic to Rutherford scattering cross sections [30, 41]. At the backward angle ($\theta = \pi$), this ratio is expressed within the semi-classical perturbation method as

$$\frac{\mathrm{d}\sigma_{\mathrm{el}}}{\mathrm{d}\sigma_{\mathrm{R}}}(E_{\mathrm{cm}}, B) = \left(1 + \frac{V_{\mathrm{N}}(R_{\mathrm{C}})}{E_{\mathrm{cm}}}\sqrt{\frac{Z_1 Z_2}{E_{\mathrm{cm}}}\frac{\pi}{a}}\right) \frac{\exp\left|-\frac{2\pi}{\hbar\omega}(E_{\mathrm{cm}} - B)\right|}{1 + \exp\left|-\frac{2\pi}{\hbar\omega}(E_{\mathrm{cm}} - B)\right|}, \tag{20}$$

where $V_{\mathrm{N}}(R_{\mathrm{C}})$ is the nuclear potential at the Coulomb turning point $R_{\mathrm{C}} = \frac{Z_1 Z_2 \epsilon^2}{E_{\mathrm{cm}}}$. The scattering parameter is $a = 0.75$, and E_{cm} and $\hbar\omega$ are the center-of-mass energy and barrier curvature, respectively. The correction term P_{corr} in Eq. (19) accounts for nucleon transfer effects in quasi-elastic scattering [42].

4. Results and discussion

In this study, we examined different versions of the proximity potential for the following reactions:

$$^{16}\mathrm{O} + {}^{64}\mathrm{Zn}\,, \quad {}^{16}\mathrm{O} + {}^{92}\mathrm{Zr}\,, \quad {}^{16}\mathrm{O} + {}^{116}\mathrm{Sn}\,, \quad {}^{16}\mathrm{O} + {}^{144}\mathrm{Sm}\,, \quad {}^{16}\mathrm{O} + {}^{154}\mathrm{Sm}\,,$$
$$^{16}\mathrm{O} + {}^{186}\mathrm{W}\,, \quad {}^{16}\mathrm{O} + {}^{208}\mathrm{Pb}\,, \quad {}^{32}\mathrm{S} + {}^{110}\mathrm{Pd}\,.$$

Experimental data for fusion and quasi-elastic cross sections of these reactions are available in Refs. [48–50]. The total interaction potential is obtained by summing the nuclear and Coulomb potentials

$$V_{\mathrm{tot}}(r) = V_{\mathrm{N}}(r) + V_{\mathrm{C}}(r) = V_{\mathrm{N}}(r) + \frac{Z_1 Z_2 e^2}{r}\,, \tag{21}$$

where Z_1 and Z_2 are the atomic numbers of the interacting nuclei. The barrier position R_{B} and height V_{B} are determined by the conditions

$$\left(\frac{\mathrm{d}V_{\mathrm{tot}}(r)}{\mathrm{d}r}\right)_{r=R_{\mathrm{B}}} = 0\,, \qquad \left(\frac{\mathrm{d}^2 V_{\mathrm{tot}}(r)}{\mathrm{d}^2 r}\right)_{r=R_{\mathrm{B}}} \leq 0\,. \tag{22}$$

Knowledge of the potential shape and the parameters R_{B} and V_{B} allow us to calculate theoretical fusion cross sections using Eqs. (9)–(19). The input parameters for calculating fusion and quasi-elastic scattering cross sections are listed in Table 2. Since barrier height and position are not directly measured, they are not ideal for assessing potential accuracy. Therefore, we evaluate the accuracy using the average relative errors for fusion $\chi^2_{\mathrm{R}}(\mathrm{fus})$ and quasi-elastic $\chi^2_{\mathrm{R}}(\mathrm{qel})$ cross sections

$$\chi^2_{\mathrm{R}}(\mathrm{fus}) = \frac{1}{N}\sum_{i=1}^{N}\left(\frac{\sigma_{\mathrm{fus}}^{\mathrm{theory}} - \sigma_{\mathrm{fus}}^{\mathrm{exp}}}{\sigma_{\mathrm{fus}}^{\mathrm{theory}} + \sigma_{\mathrm{fus}}^{\mathrm{exp}}}\right)^2, \tag{23}$$

$$\chi^2_{\mathrm{R}}(\mathrm{qel}) = \frac{1}{N}\sum_{i=1}^{N}\left(\frac{\sigma_{\mathrm{qel}}^{\mathrm{theory}} - \sigma_{\mathrm{qel}}^{\mathrm{exp}}}{\sigma_{\mathrm{qel}}^{\mathrm{theory}} + \sigma_{\mathrm{qel}}^{\mathrm{exp}}}\right)^2, \tag{24}$$

where N is the number of reactions. The computed average relative errors (χ^2) are reported in Fig. 1. It is evident that subversion 10, with $\gamma_0 = 1.08948$ MeV/fm^2 and $k_s = 1.9830$, yields the smallest χ^2 values among all subversions.

Table 2. The input parameters of the fusion barriers and quasi-elastic scattering cross section for subversion 10.

Reactions	B_0	R_0	$\hbar w$
$^{16}O + ^{64}Zn$	34.714	9.250	2.503
$^{16}O + ^{92}Zr$	43.877	9.750	3.173
$^{16}O + ^{116}Sn$	52.977	10.000	3.970
$^{16}O + ^{144}Sm$	63.490	10.500	3.953
$^{16}O + ^{154}Sm$	62.606	10.500	4.316
$^{16}O + ^{186}W$	72.397	11.0	4.194
$^{16}O + ^{208}Pb$	78.649	11.25	4.275
$^{32}S + ^{110}Pd$	93.244	10.50	5.380

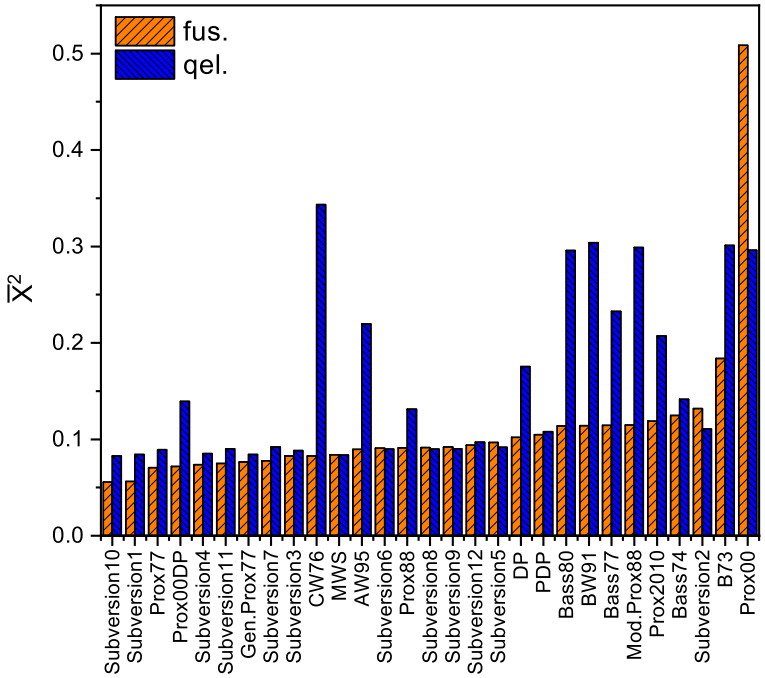

Fig. 1. The sorted average values of χ^2 based on different proximity potentials and subversions for fusion (fus.) and quasi-elastic (qel.) scattering cross sections.

According to Fig. 1, all proximity versions studied describe fusion cross sections systematically better than quasi-elastic cross sections. Another notable result is that the minimum average χ^2 values for both fusion and quasi-elastic scattering cross sections correspond to subversion 10. To better understand the deviations for each reaction, the χ^2 values are provided in Tables 3 and 4.

Table 3. The χ^2 values of fusion cross section of each of reactions for different theoretical models.

Model	$^{16}O + ^{64}Zn$	$^{16}O + ^{92}Zr$	$^{16}O + ^{116}Sn$	$^{16}O + ^{144}Sm$	$^{16}O + ^{154}Sm$	$^{16}O + ^{186}W$	$^{16}O + ^{208}Pb$	$^{32}S + ^{110}Pd$
Prox00DP	0.0745	0.0388	0.0574	0.1106	0.1578	0.0451	0.005	0.0863
AW95	0.0588	0.0167	0.0173	0.0861	0.2337	0.0733	0.0071	0.2248
Bass73	0.0646	0.1983	0.2212	0.1863	0.1776	0.1131	0.0808	0.4299
Bass74	0.0122	0.0997	0.1479	0.1209	0.1578	0.0626	0.0372	0.3608
Bass77	0.0715	0.0767	0.0149	0.0317	0.268	0.1679	0.0649	0.2209
Bass80	0.0703	0.0664	0.0329	0.1106	0.2336	0.1142	0.0106	0.2717
BW91	0.1006	0.1118	0.0088	0.047	0.2391	0.1455	0.0198	0.2411
CW76	0.1497	0.0288	0.0092	0.1043	0.2301	0.0099	0.0395	0.0906
DP	0.0541	0.0523	0.0373	0.1015	0.2119	0.0733	0.0026	0.2828
Gen.prox77	0.1233	0.0436	0.0295	0.0675	0.2008	0.0307	0.0054	0.1104
Mod.prox88	0.1121	0.0459	0.0106	0.0788	0.2795	0.0862	0.016	0.2885
MWS	0.0896	0.0362	0.0355	0.0884	0.1837	0.0252	0.0106	0.2039
P00	0.4541	0.4886	0.4957	0.5186	0.6272	0.6153	0.5415	0.3286
Prox2010	0.119	0.0889	0.0163	0.0407	0.2494	0.1795	0.0678	0.1899
Prox77	0.1384	0.0153	0.035	0.0777	0.1759	0.0149	0.0168	0.0904
Prox88	0.1209	0.0212	0.0073	0.0794	0.235	0.0527	0.014	0.1972
PDP	0.1404	0.1321	0.0077	0.0587	0.2747	0.1098	0.0261	0.0895
Subversion1	0.1024	0.0106	0.0695	0.1097	0.1082	0.0025	0.0214	0.0257
Subversion2	0.0055	0.098	0.212	0.2658	0.0239	0.1214	0.1285	0.2006
Subversion3	0.0345	0.0459	0.1504	0.2081	0.0271	0.0565	0.0786	0.0596
Subversion4	0.0507	0.0238	0.1307	0.188	0.0404	0.0425	0.0697	0.0449
Subversion5	0.027	0.0651	0.1658	0.2241	0.0137	0.0885	0.1013	0.0887
Subversion6	0.0318	0.055	0.1583	0.2165	0.017	0.0781	0.0946	0.0748
Subversion7	0.1395	0.0203	0.0308	0.0687	0.2019	0.0338	0.0208	0.1073
Subversion8	0.0318	0.0554	0.1588	0.2171	0.0163	0.0805	0.0964	0.0753
Subversion9	0.0312	0.0566	0.1596	0.2179	0.016	0.0812	0.0967	0.0767
Subversion10	0.0785	0.0036	0.1077	0.1485	0.0492	0.0109	0.041	0.0074
Subversion11	0.1564	0.0276	0.0276	0.0644	0.1785	0.014	0.0169	0.1144
Subversion12	0.1623	0.0461	0.0184	0.0448	0.2309	0.0596	0.0313	0.1578

Table 4. The χ^2 values of quasi-elastic scattering cross section of each of reactions for different theoretical models.

Model	$^{16}O + ^{64}Zn$	$^{16}O + ^{92}Zr$	$^{16}O + ^{116}Sn$	$^{16}O + ^{144}Sm$	$^{16}O + ^{154}Sm$	$^{16}O + ^{186}W$	$^{16}O + ^{208}Pb$	$^{32}S + ^{110}Pd$
Prox00DP	0.004	0.512	0.2571	0.1189	0.0686	0.0345	0.0472	0.0736
AW95	0.0357	0.5947	0.3203	0.1947	0.1878	0.0966	0.1472	0.1811
Bass73	0.3088	0.7288	0.4689	0.2965	0.2766	0.108	0.1186	0.1027
Bass74	0.106	0.5864	0.285	0.0763	0.035	0.0055	0.0368	0.002
Bass77	0.0414	0.6044	0.3291	0.2015	0.198	0.0974	0.1454	0.2449
Bass80	0.0638	0.6356	0.3732	0.2842	0.2772	0.1649	0.2747	0.2917
BW91	0.0655	0.6414	0.3703	0.2922	0.284	0.1654	0.2915	0.3216
CW76	0.1403	0.656	0.4363	0.3232	0.3472	0.1832	0.3115	0.3502
DP	0.0196	0.5605	0.2937	0.1593	0.1253	0.0624	0.0825	0.0999
Gen.prox77	0.0048	0.4266	0.1763	0.0229	0.0053	0.0025	0.0286	0.0082
Mod.prox88	0.0888	0.6418	0.3775	0.2802	0.2814	0.154	0.2732	0.2944
MWS	9E-4	0.4271	0.1776	0.0246	0.0051	0.0022	0.0298	0.0015
Prox00	0.0814	1.3546	0.1521	0.1328	0.2019	0.1269	0.2875	0.0326
Prox2010	0.0301	0.5844	0.3011	0.1868	0.1579	0.0861	0.1388	0.1727
Prox77	0.0102	0.4626	0.1404	0.0055	0.0218	0.0074	0.0626	0.004
Prox88	0.0047	0.4925	0.2464	0.0963	0.0625	0.0309	0.0503	0.0663
PDP	0.0106	0.4307	0.1969	0.0334	0.0306	0.0281	0.113	0.0202
Subversion1	0.0061	0.443	0.1501	0.0085	0.011	0.0035	0.0486	0.0027
Subversion2	0.0033	0.0086	0.0201	0.0162	0.0029	0.0041	0.0017	0.0167
Subversion3	1E-4	0.4338	0.1906	0.0376	0.0029	0.0024	0.0179	0.021
Subversion4	4E-4	0.4316	0.1811	0.028	0.0024	0.0015	0.0211	0.0163
Subversion5	3E-4	0.4374	0.1992	0.0474	0.0054	0.0056	0.0115	0.0278
Subversion6	1E-4	0.4353	0.1949	0.0425	0.0043	0.0044	0.0131	0.0243
Subversion7	0.0103	0.4665	0.1388	0.0052	0.027	0.0108	0.0745	0.0046
Subversion8	1E-4	0.4354	0.1951	0.0428	0.0045	0.0046	0.0126	0.0246
Subversion9	1E-4	0.4357	0.1956	0.0434	0.0046	0.0047	0.0126	0.025
Subversion10	0.0021	0.4343	0.1631	0.0154	0.0045	0.0013	0.0345	0.0059
Subversion11	0.0124	0.4717	0.1378	0.0051	0.0223	0.0072	0.0607	0.005
Subversion12	0.0132	0.4835	0.1348	0.0054	0.0335	0.0146	0.0849	0.0071

To illustrate the energy-dependent behavior of fusion and quasi-elastic scattering cross sections based on the barrier distribution approach, we compare theoretical models (Prox77, Prox2010, Prox88, PDP, CW76, Bass80, Bass77, and subversion 10) with experimental data for the reactions $^{16}O + ^{92}Zr$ and $^{32}S + ^{110}Pd$ in Fig. 2. The figure shows acceptable agreement between our results and experimental data. However, for the $^{32}S + ^{110}Pd$ reaction, the calculated values overestimate the experimental data, likely due to significant nuclear transfer effects in this reaction [52].

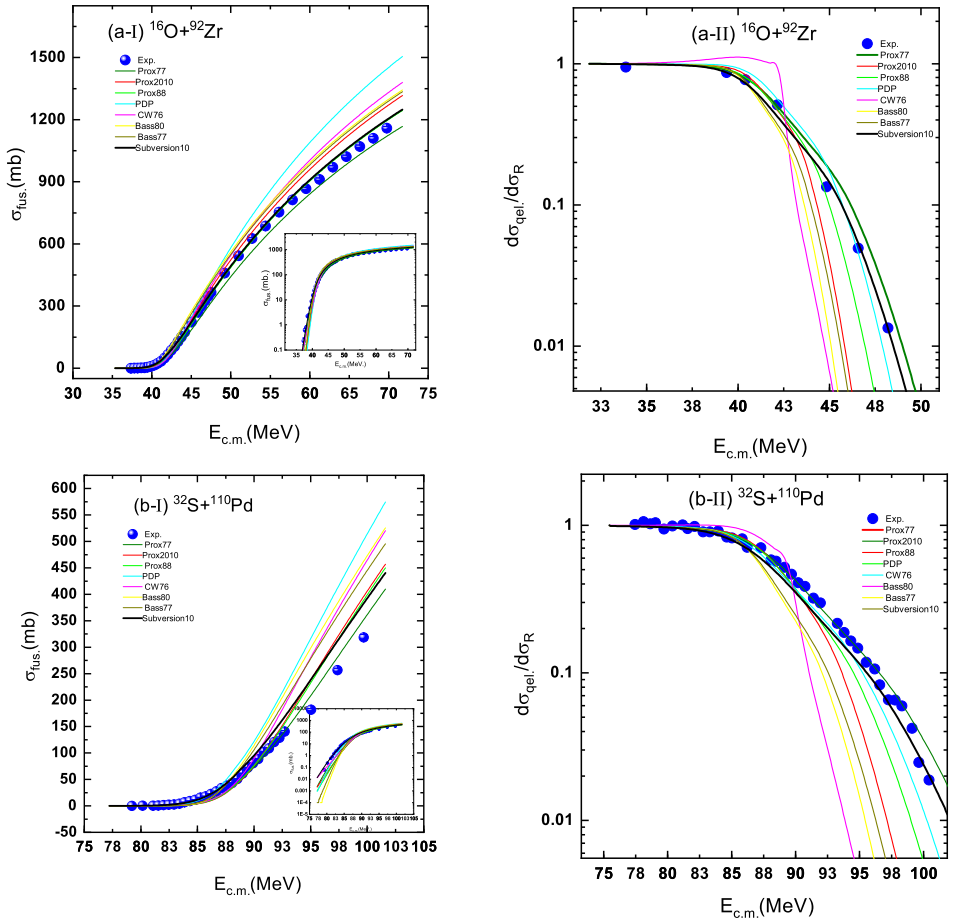

Fig. 2. Comparison of the fusion (left) and ratio of quasi-elastic-to-Rutherford (right) cross sections with experimental data.

Based on the above results, theoretical values of fusion and the quasi-elastic-to-Rutherford cross-section ratio from subversion 10 are compared with experimental data in Figs. 3 and 4. Additionally, panel (c-1) of Fig. 4 displays the fusion barrier distribution for ^{16}O + ^{208}Pb calculated using the present method as an example. In Fig. 3 (b-1) for the ^{16}O + ^{116}Sn reaction, a discrepancy between predictions and experimental data is observed. This is because the average barrier height calculated by subversion 10 (50.573947 MeV) is lower than both the experimental value (52.977657 MeV) and the SAGBD calculation (53.65 MeV) [53], leading to an overestimation of the fusion cross section. Moreover, ^{16}O+^{116}Sn are double closed-shell nuclei, considered stiff, which may require adjustments in the EBDM method used for such systems.

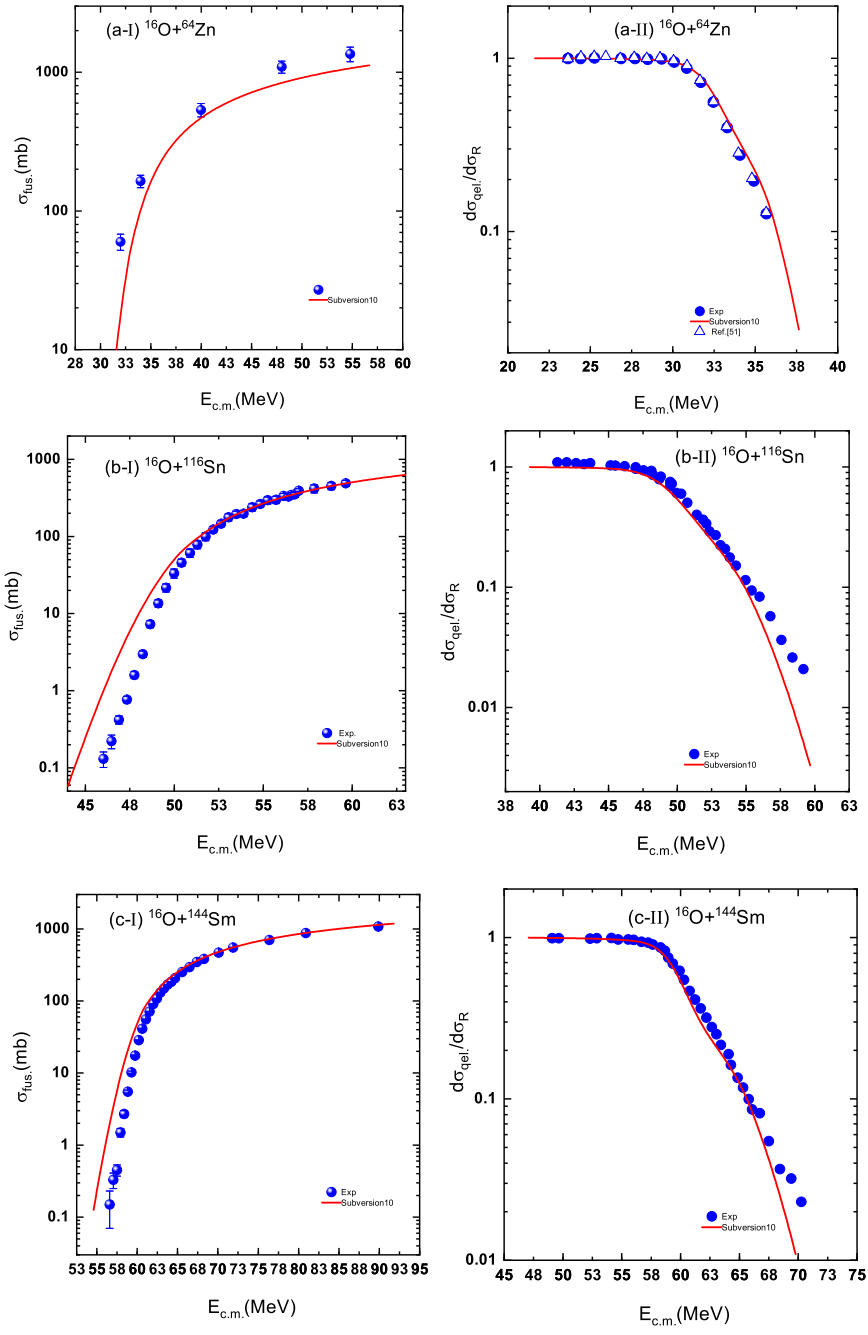

Fig. 3. The same as Fig. 2 — comparison of the obtained results of the subversion 10 with experimental data.

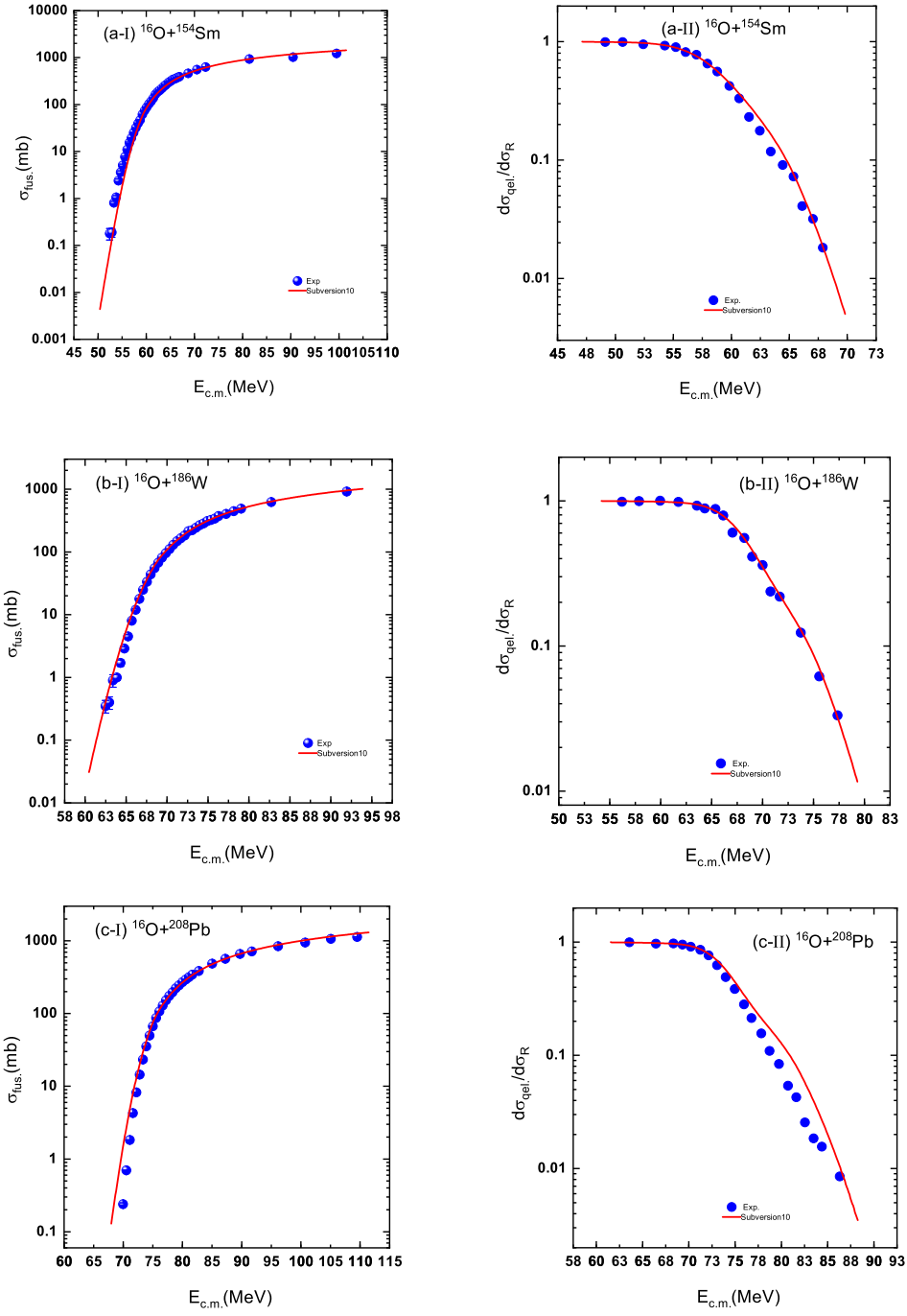

Fig. 4. Continuation of Fig. 3.

To demonstrate the role of the total interaction potential and the surface energy coefficient, we plot the total potential for different subversions. The results for $^{16}O + ^{208}Pb$ are shown in Fig. 5. As seen, increasing γ_0 enhances the attractive nuclear potential component, which can dominate the repulsive Coulomb force.

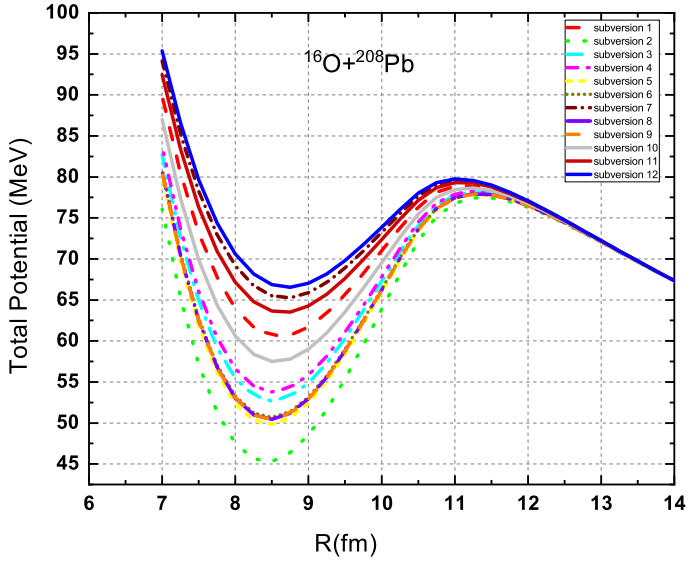

Fig. 5. Total potential as a distance for the $^{16}O + ^{208}Pb$ reaction using different subversions of proximity 1977.

Figure 6 compares the total interaction potential as a function of the internuclear distance for the $^{16}O + ^{208}Pb$ system, calculated using various theoretical models (*e.g.*, Prox77, Prox88, Bass80, *etc.*) and subversion 10 of the Prox77 potential. The subversion 10 potential exhibits a stronger attractive nuclear component at intermediate distances compared to other models. This enhanced attraction leads to a lower and broader barrier, which is crucial for reproducing both fusion and quasi-elastic scattering data. The proximity of the subversion 10 curve to the expected phenomenological behavior underscores its suitability for a unified description of heavy-ion reactions near the Coulomb barrier.

Finally, Fig. 7 presents fusion barrier distributions for the (a) $^{16}O + ^{92}Zr$ and (b) $^{16}O + ^{208}Pb$ systems using subversion 10 of the Prox77 potential compared with experimental data. The barrier distribution, extracted from the second derivative of the excitation function, reflects the coupling of internal degrees of freedom (such as deformations and vibrations) to the relative motion. For both systems, the subversion 10 results closely follow the experimental trends, capturing the peak positions and widths of the distributions.

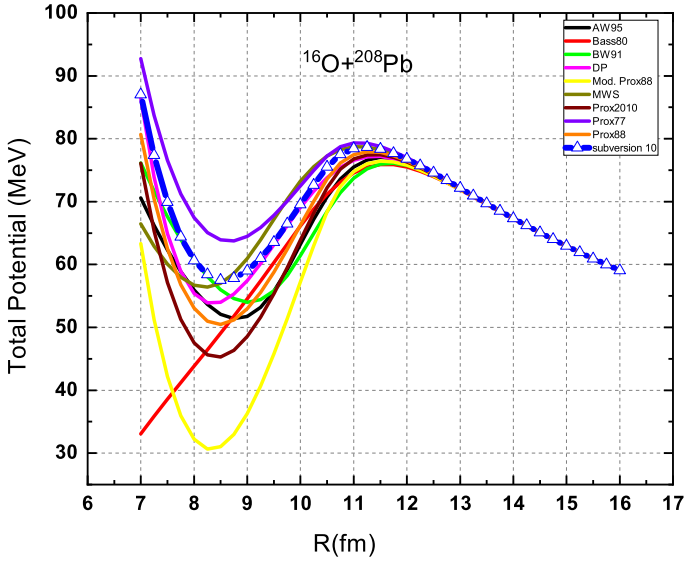

Fig. 6. Total potential as a radius for the $^{16}\mathrm{O} + {}^{208}\mathrm{Pb}$ reaction using different theoretical models and subversion10.

The narrower distribution for $^{16}\mathrm{O} + {}^{208}\mathrm{Pb}$ indicates weaker coupling effects, whereas the broader distribution for $^{16}\mathrm{O} + {}^{92}\mathrm{Zr}$ suggests stronger structural couplings. The agreement demonstrates that subversion 10, with its optimized surface parameters, reliably accounts for the dynamic effects that govern both fusion and quasi-elastic scattering cross sections.

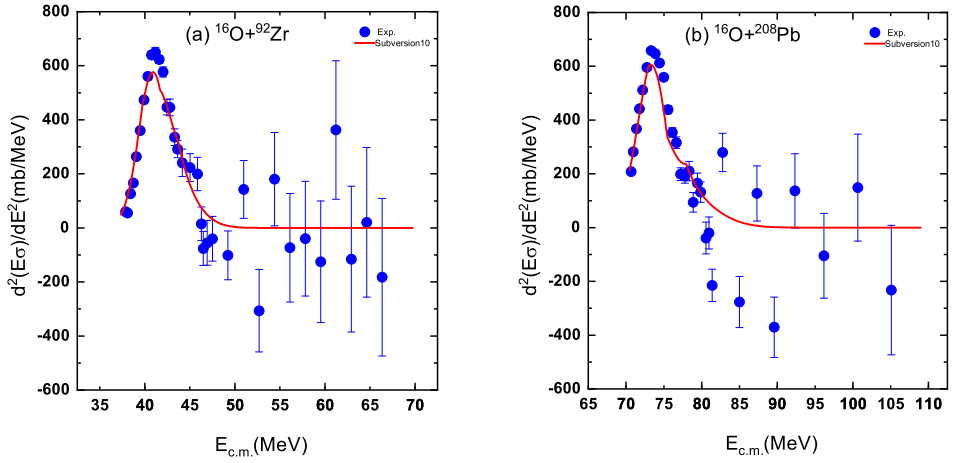

Fig. 7. The calculated barrier distributions of the (a) $^{16}\mathrm{O}+{}^{92}\mathrm{Zr}$ and (b) $^{16}\mathrm{O}+{}^{208}\mathrm{Pb}$ systems. In these calculations, it has been assumed that $\Delta E = 2.0$ MeV.

5. Conclusions

In this work, we investigated the influence of the surface energy constant (γ_0) and surface asymmetry constant (k_s) on fusion and quasi-elastic scattering cross sections simultaneously. The nuclear potential was studied using the Prox77 model with different sets of γ and k parameters. This study identifies which parameter set can most accurately describe both fusion and quasi-elastic cross sections concurrently. Our comparison with available experimental data indicates that subversion 10, with parameters $\gamma_0 = 1.08948$ MeV/fm^2 and $k_s = 1.9830$, explains the fusion excitation function and quasi-elastic scattering with average deviation errors χ^2 of 0.0558 and 0.0826, respectively.

REFERENCES

[1] A. Yadav *et al.*, «Effect of entrance-channel parameters on incomplete fusion reactions», *Phys. Rev. C* **85**, 064617 (2012).

[2] Muhammad Zamrun F., K. Hagino, S. Mitsuoka, H. Ikezoe, «Coupled-channels analyses for large-angle quasi-elastic scattering in massive systems», *Phys. Rev. C* **77**, 034604 (2008).

[3] K. Hagino, N. Rowley, «Large-angle scattering and quasielastic barrier distributions», *Phys. Rev. C* **69**, 054610 (2004).

[4] J.O. Newton *et al.*, «Systematic failure of the Woods–Saxon nuclear potential to describe both fusion and elastic scattering: Possible need for a new dynamical approach to fusion», *Phys. Rev. C* **70**, 024605 (2004).

[5] C.H. Rong *et al.*, «Study of quasi-elastic scattering of ^{17}F + ^{208}Pb at energies around Coulomb barrier», *Eur. Phys. J. A* **57**, 143 (2021).

[6] H. Timmers *et al.*, «Probing fusion barrier distributions with quasi-elastic scattering», *Nucl. Phys. A* **584**, 190 (1995).

[7] N. Wang, W. Scheid, «Quasi-elastic scattering and fusion with a modified Woods–Saxon potential», *Phys. Rev. C* **78**, 014607 (2008).

[8] S. Mittal, I. Dutt, «The systematic study of N/Z dependence on surface diffuseness parameter in the fusion of heavy neutron-rich colliding nuclei», *AIP Conf. Proc.* **1728**, 020143 (2016).

[9] Rajni, M.K. Sharma, «Influence of nuclear surface diffuseness on systems involving spherical and deformed targets», *Int. J. Mod. Phys. E* **28**, 1950052 (2019).

[10] J. Błocki, J. Randrup, W.J. Świątecki, C.F. Tsang, «Proximity forces», *Ann. Phys.* **105**, 427 (1977).

[11] I. Dutt, R.K. Puri, «Comparison of different proximity potentials for asymmetric colliding nuclei», *Phys. Rev. C* **81**, 064609 (2010).

[12] I. Dutt, R.K. Puri, «Systematic study of the fusion barriers using different proximity-type potentials for $N = Z$ colliding nuclei: New extensions», *Phys. Rev. C* **81**, 044615 (2010).

[13] K.P. Santhosh, V. Bobby Jose, «Heavy-ion fusion cross sections of weakly bound ^{9}Be on ^{27}Al, ^{64}Zn and tightly bound ^{16}O on ^{64}Zn target using Coulomb and proximity potential», *Nucl. Phys. A* **922**, 191 (2014).

[14] K.P. Santhosh, V. Bobby Jose, «Heavy-ion fusion reactions of ^{16}O on spherical/deformed $^{144-154}$Sm targets using coulomb and proximity potentials», *Rom. Rep. Phys.* **66**, 939 (2014).

[15] V. Zanganeh, R. Gharaei, A.M. Izadpanah, «Comparative study for different nuclear proximity potentials applied to quasi-elastic scattering and fusion reactions», *Nucl. Phys. A* **992**, 121637 (2019).

[16] W. Reisdorf, «Heavy-ion reactions close to the Coulomb barrier», *J. Phys. G: Nucl. Part. Phys.* **20**, 1297 (1994).

[17] W.D. Myers, W.J. Świątecki, «Nucleus–nucleus proximity potential and superheavy nuclei», *Phys. Rev. C* **62**, 044610 (2000).

[18] W.D. Myers, W.J. Świątecki, «Average nuclear properties», *Ann. Phys.* **55**, 395 (1969); «Droplet-model theory of the neutron skin», *Nucl. Phys. A* **336**, 267 (1980).

[19] A.M. Stefanini *et al.*, «Fusion of the positive Q-value system ^{36}S + ^{48}Ca well below the Coulomb barrier», *Phys. Rev. C* **78**, 044607 (2008).

[20] G. Royer, R. Rousseau, «On the liquid drop model mass formulae and charge radii», *Eur. Phys. J. A* **42**, 541 (2009).

[21] R. Bass, «Threshold and angular momentum limit in the complete fusion of heavy ions», *Phys. Lett. B* **47**, 139 (1973).

[22] R. Bass, «Nucleus–Nucleus Potential Deduced from Experimental Fusion Cross Sections», *Phys. Rev. Lett.* **39**, 265 (1977).

[23] R. Bass, «Fusion of heavy nuclei in a classical model», *Nucl. Phys. A* **231**, 45 (1974).

[24] P.R. Christensen, A. Winther, «The evidence of the ion–ion potentials from heavy ion elastic scattering», *Phys. Lett. B* **65**, 19 (1976).

[25] A. Winther, «Dissipation, polarization and fluctuation in grazing heavy-ion collisions and the boundary to the chaotic regime», *Nucl. Phys. A* **594**, 203 (1995).

[26] C. Ngô *et al.*, «Properties of heavy ion interaction potentials calculated in the energy density formalism», *Nucl. Phys. A* **252**, 237 (1975).

[27] H. Ngô, Ch. Ngô, «Calculation of the real part of the interaction potential between two heavy ions in the sudden approximation», *Nucl. Phys. A* **348**, 140 (1980).

[28] V.Y. Denisov, «Interaction potential between heavy ions», *Phys. Lett. B* **526**, 315 (2002).

[29] C.Y. Wong, «Interaction Barrier in Charged-Particle Nuclear Reactions», *Phys. Rev. Lett.* **31**, 766 (1973).

[30] P.H. Stelson, «Neutron flow between nuclei as the principal enhancement mechanism in heavy-ion subbarrier fusion», *Phys. Lett. B* **205**, 190 (1988).

[31] W.D. Myers, W.J. Świątecki, «Anomalies in nuclear masses», *Ark. Fys.* **36**, 343 (1967).

[32] W.D. Myers, W.J. Świątecki, «Nuclear masses and deformations», *Nucl. Phys.* **81**, 1 (1966).

[33] P. Möller, J.R. Nix, «Macroscopic potential-energy surfaces for symmetric fission and heavy-ion reactions», *Nucl. Phys. A* **272**, 502 (1976).

[34] H.J. Krappe, J.R. Nix, A.J. Sierk, «Unified nuclear potential for heavy-ion elastic scattering, fusion, fission, and ground-state masses and deformations», *Phys. Rev. C* **20**, 992 (1979).

[35] P. Möller, J.R. Nix, «Nuclear mass formula with a Yukawa-plus-exponential macroscopic model and a folded-Yukawa single-particle potential», *Nucl. Phys. A* **361**, 117 (1981).

[36] G. Royer, B. Remaud, «Fission processes through compact and creviced shapes», *J. Phys. G: Nucl. Part. Phys.* **10**, 1057 (1984).

[37] P. Möller, J.R. Nix, «Nuclear masses from a unified macroscopic–microscopic model», *At. Data Nucl. Data Tables* **39**, 213 (1988).

[38] P. Möller, J.R. Nix, W.D. Myers, W.J. Świątecki, «Nuclear Ground-State Masses and Deformations», *Atom. Data Nucl. Data Tables* **59**, 185 (1995).

[39] K. Pomorski, J. Dudek, «Nuclear liquid-drop model and surface-curvature effects», *Phys. Rev. C* **67**, 044316 (2003).

[40] W.D. Myers, W.J. Swiatecki, «Nuclear masses and deformations», *Nucl. Phys.* **81**, 1 (1966).

[41] N. Wang, Z. Li, W. Scheid, «Systematic study of fusion barriers», *J. Phys. G: Nucl. Part. Phys.* **34**, 1935 (2007).

[42] M. Liu *et al.*, «Applications of Skyrme energy-density functional to fusion reactions spanning the fusion barriers», *Nucl. Phys. A* **768**, 80 (2006).

[43] K. Hagino, N. Rowley, «Large-angle scattering and quasielastic barrier distributions», *Phys. Rev. C* **69**, 054610 (2004).

[44] C.C. Sahm *et al.*, «Total reaction cross section for ^{12}C on ^{12}C, ^{40}Ca, ^{90}Zr, and ^{208}Pb between 10 and 35 MeV/nucleon», *Phys. Rev. C* **34**, 2165 (1986).

[45] J.O. Newton *et al.*, «Systematic failure of the Woods–Saxon nuclear potential to describe both fusion and elastic scattering: Possible need for a new dynamical approach to fusion», *Phys. Rev. C* **70**, 024605 (2004).

[46] A.T. Kruppa, E. Romain, M.A. Nagarajan, N. Rowley, «Effect of multiphonon coupling on heavy-ion fusion», *Nucl. Phys. A* **560**, 845 (1993).

[47] M.V. Andres, N. Rowley, M.A. Nagarajan, «Effect of deformation on the elastic and quasielastic scattering of heavy ions near the Coulomb barrier», *Phys. Lett. B* **202**, 292 (1988).

[48] J.R. Leigh *et al.*, «Barrier distributions from the fusion of oxygen ions with ^{144,148,154}Sm and ^{186}W», *Phys. Rev. C* **52**, 3151 (1995).

[49] H. Timmers *et al.*, «Probing fusion barrier distributions with quasi-elastic scattering», *Nucl. Phys. A* **584**, 190 (1995).

[50] `http://nrv.jinr.ru/nrv/`

[51] J.F.P. Huiza *et al.*, «Simultaneous analysis of quasielastic, elastic, and inelastic scattering and of fusion in the $^{16}O + ^{64}Zn$ system», *Phys. Rev. C* **75**, 064601 (2007).

[52] O.A. Capurro *et al.*, «Barrier distribution for the $^{32}S + ^{110}Pd$ system derived from the quasielastic scattering excitation function», *Phys. Rev. C* **61**, 037603 (2000).

[53] V. Ghanghas *et al.*, «Interplay of Neutron Transfer in the Fusion Process of $^{16}O + ^{112,116,120}Sn$ and $^{18}O + ^{116}Sn$ Systems at Sub-barrier Energies», *Braz. J. Phys.* **52**, 84 (2022).